HHS Public Access

Author manuscript

AJR Am J Roentgenol. Author manuscript; available in PMC 2017 September 01.

Published in final edited form as:

AJR Am J Roentgenol. 2017 September ; 209(3): 534–543. doi:10.2214/AJR.16.17789.

Advanced MRI Techniques for the Hip Joint: Focus on the Postoperative Hip

Jennifer L. Berkowitz[1] and **Hollis G. Potter**

[1]Department of Radiology and Imaging, Hospital for Special Surgery, 535 East 70th St, New York, NY 10021

Abstract

OBJECTIVE—Imaging the hip joint with optimized MRI protocol parameters provides the radiologist with the ability to reliably diagnose complex hip abnormalities. The institution of appropriate metal artifact reduction techniques and dedicated sequences can enhance visualization of the periprosthetic bone and soft tissues and allow improved detection of the more frequently encountered total hip arthroplasty–related conditions, such as mechanical loosening, polyethylene wear, and adverse local tissue reactions.

CONCLUSION—Finally, through the use of dynamic contrast-enhanced MRI, abnormal femoral head perfusion, one of the most common complications associated with femoral neck fracture internal fixation, can be detected before the development of femoral head osteonecrosis, subchondral collapse, and secondary osteoarthritis. Thus, through the institution of the techniques described in this review article, the challenges associated with MRI of hip arthroplasty and instrumentation can be overcome, allowing for the diagnosis of common associated complications.

Keywords

arthroplasty; hip; MRI

Accurate evaluation of the hip joint is integral to identifying complex hip abnormalities, aiding in preoperative and pre-arthroscopic procedure planning, and assessing for postoperative complications. Although the anatomic location of the hip off isocenter of the imaging bore, as well as the sphericity of the femoral head and relatively thin femoral head and acetabular dome articular cartilage, present challenges to assessing the hip joint with the use of MRI, the use of proper pulse sequence protocols can overcome these challenges.

Furthermore, approximately 2.5 million Americans currently live with a hip arthroplasty [1], and this number is expected to increase in the coming decades, given the increased life expectancy of the aging population, as well as the movement toward hip replacement in younger patients. Although hip arthroplasty provides patients with pain relief and improved subjective function, it is also associated with several complications that can limit arthroplasty's life span, for which it is integral for imaging to be able to evaluate. In the past, the use of MRI to assess hip arthroplasty had been limited because of metal-related artifact;

Address correspondence to J. L. Berkowitz (berkowitzj@hss.edu).

however, in recent years, protocols and sequences geared toward reducing such artifacts have rendered MRI instrumental in assessing hip arthroplasty–related complications, such as mechanical loosening, polyethylene wear, and adverse local tissue reactions.

The intent of this article is to outline the techniques that can be used to overcome the challenges associated with MRI of hip arthroplasty, as well as the typical MRI features of common hip arthroplasty–associated complications.

Routine Imaging Technique

Hip MRI is ideally performed on a 1.5- or 3-T magnet. Coronal, sagittal, and axial high-resolution surface coil images should be obtained with a two-part shoulder smaller-FOV wrap or multiple-channel cardiac coil to avoid phase-wrap artifact, which would result from the use of a larger-FOV body coil. Cartilage-sensitive moderate-TE fast spin-echo (FSE) sequences with an effective TE of approximately 34 ms at 1.5 T, or 28 ms at 3 T, should be acquired in an effort to maximize the contrast between the hypointense fibrocartilaginous labrum, isointense articular cartilage, and hyperintense fluid. Larger-FOV coronal fast STIR and axial FSE sequences should also be performed using a body coil. These more global images may show alternate abnormalities that may simulate hip joint pain, such as occult sacral or pubic insufficiency fractures, pelvic soft-tissue masses (e.g., adnexal masses or hernias), or remote marrow infiltration indicative of metastatic disease.

Imaging Techniques Around Orthopedic Hardware

The challenge of arthroplasty imaging is that the magnetic susceptibility generated from the metal prosthesis alters the regional static magnetic field, thereby changing local precessional frequencies [2]. This results in field inhomogeneities that distort regional anatomy and reallocate signal from its proper position to overlie like frequency spins, generating areas of signal pileup around areas of signal loss [3, 4], with resultant misregistration artifacts in both the slice selection and readout directions during signal encoding [2, 5]. Metallic implants also accelerate proton dephasing, which degrades the periprosthetic signal [6]. Magnetic susceptibility and its associated artifact vary according to material, peaking with stainless steel and decreasing from cobalt chromium to titanium, and its associated distortion is greatest closest to the metal arthroplasty [7].

Several modifications to routine hip imaging techniques may be performed to mitigate arthroplasty-related artifacts. Imaging at 1.5 T, as opposed to 3 T, is recommended because susceptibility artifact is proportional to the applied magnetic field strength. In addition, because susceptibility artifact is inversely proportional to the magnetic field frequency-encoding and slice select gradient strengths, increasing the gradient amplitudes will decrease susceptibility artifact. Consequently, using a wider receiver bandwidth and a smaller voxel size, which minimizes variation and dephasing within a single voxel, will increase the frequency-encoding and slice select gradient amplitudes, thereby decreasing distortion and improving spatial resolution [2–4]. Moreover, adjusting the direction of the frequency-encoding gradient to run along the long axis of the arthroplasty will diminish susceptibility artifact even further [6]. In addition, using FSE imaging and its 180° refocusing pulse will

reduce signal loss from static field dephasing associated with arthroplasty imaging [5]. Finally, intermediate-weighted imaging will provide the spatial resolution, contrast-to-noise ratio, and fluid sensitivity necessary to accurately depict the periprosthetic bone, synovium, and soft tissues, as well as metallic deposits and adverse local tissue reactions [4] (Table 1).

It should be noted that a number of the aforementioned artifact reduction techniques will have downstream imaging effects. For example, a decreased signal-to-noise ratio will result from the use of a wide-readout bandwidth and thinner slices, which can be counterbalanced by increasing the number of excitations; however, this will, in turn, lengthen the scan time. On the other hand, steeper gradients will allow decreased interecho spacing and thus enable an increased echo-train length, making shorter imaging times possible, but at the cost of a decreased signal-to-noise ratio [4, 6].

Arthroplasty imaging fat suppression is more homogeneous when it is achieved through the use of STIR imaging, as opposed to frequency-selective fat suppression. Frequency-selective fat suppression takes advantage of the chemical-shift frequency differences between lipid and water and applies a saturation pulse with the same resonant frequency as fat, followed by a spoiling gradient pulse to null the signal from fat [8]; however, frequency shifts adjacent to metal alter the resonance frequency of fat, hampering frequency-selective fat suppression [5]. Inversion recovery fat suppression, on the other hand, exploits fat's short T1 relaxation time, which is insensitive to magnetic field nonuniformity. STIR imaging uses a 90° inversion pulse at the null point of fat, thereby saturating the signal generated by adipose tissue [8]. Disadvantages associated with the use of inversion recovery imaging are a diminished signal-to-noise ratio and the inability to perform contrast-enhanced imaging, because enhancing tissue is nulled along with the fat signal as a result of its shortened longitudinal recovery time [5].

In recent years, several dedicated MRI 3D multispectral imaging sequences have been generated to address metal-related artifact, including the multiacquisition variable-resonance image combination (MAVRIC) and section encoding for metal artifact correction (SEMAC) techniques, which reduce both in- and through-plane distortion [5]. MAVRIC combines multiple 3D image datasets obtained at overlapped spectral frequency bins centered about the dominant frequency of hydrogen to create a composite image with minimal artifact [9], whereas SEMAC uses section-selective 3D spin-echo images obtained with view-angle tilting to minimize in-plane displacement and two phase-encoding directions to decrease through-plane distortion [10]. Furthermore, MAVRIC SL, a fusion MAVRIC-SEMAC sequence, merges the high signal-to-noise ratio and resolution associated with the MAVRIC sequence with the slice location selectivity that accompanies the SEMAC sequence. This hybrid sequence can acquire not only proton density– and T1-weighted images but also STIR images, allowing homogeneous fat suppression in the presence of metal [3]. Cross-talk artifacts have presented a challenge when it comes to 3D multispectral imaging, because spectral overlap is necessary to reduce gaps between the aforementioned spectral frequency bins. Flexible longitudinal magnetization contrast has been introduced to address this issue and bestows the operator with the ability to select the TR, echo-train length, and flip angle, followed by an automatic distribution of spectral bins to generate the least cross-talk possible. This technique allows less-restrictive spectral bin compositions, as well as the

ability to generate T1-weighted 3D multispectral imaging, which is integral in instances where contrast enhancement is necessary, such as when evaluating for osteonecrosis or osteomyelitis [11]. These 3D multispectral imaging sequences allow better visualization of the bone-prosthesis interface and, consequently, arthroplasty component integration [4] (Fig. 1). In the presence of commonly used ceramic-backed metal implants, generally optimized FSE sequences are adequate to visualize the bone-arthroplasty interface; however, in the presence of cobalt chromium components seen in metal-on-metal or some metal-on-polyethylene devices, the 3D multispectral imaging techniques are essential for adequate visualization.

Optimized MRI around postoperative hardware in the hip also allows detection of complications after femoral neck fracture internal fixation, the most common of which is osteonecrosis of the femoral head (Fig. 2). Osteonecrosis is classically delineated on MRI by serpiginous hypointense signal with or without associated subchondral collapse or secondary osteoarthritis. However, it should be noted that these findings of osteonecrosis represent the later stages of abnormal femoral head blood flow, at a point when they are no longer reversible [6]. Reversible femoral head perfusion abnormalities have historically been assessed via radionuclide bone scintigraphy; however, in recent years, dynamic contrast-enhanced MRI and dynamic gadolinium-enhanced subtraction MRI have been used to gauge femoral head viability and perfusion before the onset of osteonecrosis or osteonecrosis [12]. These techniques have proved to be efficacious in assessing femoral head perfusion after displaced femoral neck fracture [13].

Dynamic contrast-enhanced MRI establishes abnormal femoral head blood flow via comparison of contrast-enhanced signal intensity between the affected hip and unaffected contralateral hip [12]. Unenhanced baseline imaging is obtained, followed by repetitive imaging every few seconds for a few minutes after the contrast bolus injection (Table 2). Subsequently, the signal intensity from a small ROI is collected and recorded against time, allowing signal intensity alterations after IV contrast injection and peak enhancement to be derived [14] (Fig. 3). Three main dynamic contrast enhancement curve patterns have emerged: type A curves show 25–30% decreased signal intensity on the affected side, type B curves show 30–70% reduced signal intensity on the affected side, and type C curves exhibit greater than 70% decreased signal intensity on the affected side. Studies thus far have indicated that the type C curves are at increased risk of progression to subsequent osteonecrosis [12].

Dynamic gadolinium-enhanced subtraction MRI has been found to be particularly useful when evaluating enhancement within the already hyperintense lipid-rich femoral epiphyseal bone marrow. Subtraction imaging is accomplished by obtaining contrast-enhanced images every minute for 5 minutes after the administration of IV contrast agent and then subtracting absolute pixel values from unenhanced imaging by means of customary MRI software [15].

Imaging of Arthroplasty-Associated Complications

A variety of complications have been identified in patients after hip arthroplasty. Some of the more commonly encountered postoperative abnormalities include mechanical loosening, polyethylene wear, and adverse local tissue reactions.

Periprosthetic osseous resorption leading to mechanical loosening is a well-established complication of total hip arthroplasty. It has been theorized that micromotion between the implant or cement surface and the host bone resulting from mechanical stress leads to synoviocyte dispersal along the implant-bone or cement-bone interface, causing synoviallike fibrous membrane formation and the secretion of osteoclast-stimulating cytokines, ultimately resulting in osseous resorption. A spectrum of arthroplasty integration exists and includes complete implant fixation, limited arthroplasty integration represented by fibrous membrane formation, osseous resorption, and, finally, frank component loosening. Complete osseous integration is represented by normal bone marrow signal intensity flush against the cement or arthroplasty (Fig. 4). A thin rim of intermediate signal intensity around the arthroplasty signifies fibrous membrane formation (Fig. 5), whereas osteolysis is defined by a thicker rind of intermediate signal intensity at the prosthesis-bone or cement-bone interface surrounded by a hypointense rim (Fig. 6). Finally, frank component loosening corresponds to circumferential osteolysis with or without associated altered arthroplasty alignment or subsidence [4]. The implementation of the aforementioned metal artifact reduction techniques and dedicated MRI sequences afford improved visualization of the bone-implant interface and, consequently, hip arthroplasty component integration, which may allow early diagnosis and treatment and result in superior patient outcomes [6].

The most common reason for gradual metal-on-polyethylene and ceramic-on-polyethylene hip arthroplasty failure is polyethylene wear. Wear of the acetabular polyethylene liner releases polymeric debris into the joint, resulting in synovitis, increased osteoclastic and decreased osteoblastic activity, and, eventually, bulky osteolysis and implant loosening. MRI features of polyethylene wear include pseudocapsular distention by a thickened isointense-to-hyperintense synovium associated with intermediate-intensity debris, which often decompresses into the greater trochanteric, iliopsoas, and subiliacus bursae. Ultimately, the intermediate intensity particulate debris creates a cytokine-mediated process of periprosthetic bone resorption in the form of a bulky osteolysis [16] (Fig. 7). Intermediate-weighted MRI sequences are vital to detecting the intermediate-intensity particulate debris associated with polyethylene wear.

Metal arthroplasty–associated complications, including metallosis, aseptic lymphocytic vasculitis–associated lesions, and trunnionosis, have been termed adverse local tissue reactions. These reactions are thought to result from hypersensitivity to metallic debris, metal ions, or corrosion products generated by implant-related wear. Greater wear has been found to be associated with increased edge loading, which may result from a shallow acetabular cup or abnormal acetabular cup inclination [17].

Metallosis is associated with above-average metal implant wear, resulting in elevated levels of blood metal ions and a resultant foreign body reaction. MRI shows hypointense intra- or

extracapsular metallic debris, hypointense thickened synovium, hypointense osteolysis, and eventual mechanical loosening without features of aggressive surrounding soft-tissue destruction [4] (Fig. 8).

Aseptic lymphocytic vasculitis–associated lesion describes a type IV hypersensitivity reaction to metal, which is most commonly not associated with a high metal implant wear rate. Histologic evaluation of aseptic lymphocytic vasculitis–associated lesion shows metallic debris, corrosion products, lymphocytic infiltrates, and tissue necrosis [18]. Characteristic MRI features include hyperintense synovitis and debris, cystic or solid soft-tissue deposits, and extensive extracapsular regional soft-tissue damage with dehiscence of the anterior and posterior pseudocapsule and decompression into the adjacent iliopsoas, subiliacus, and greater trochanteric bursae [4] (Fig. 9). Nawabi et al. [19] found that increased synovial thickening (median, 12 mm) and a combination of solid and fluid-based synovitis strongly correlated with moderate-to severe aseptic lymphocytic vasculitis–associated lesions. They also found that solid and fluid-based synovitis, pseudocapsular disruption, and synovial decompression into the surrounding bursae were 90% sensitive and 86% specific for predicting intraoperative tissue damage, which is much more reliable than serum ion levels [19].

Trunnion corrosion, also referred to as trunnionosis, reflects a soft-tissue reaction to metal by-products released from micromotion and mechanical wear at the head-neck or neck-stem junctions of mixed alloy modular metal-on-polyethylene arthroplasties [17, 20, 21]. An adverse local tissue reaction has been found to result in synovitis, debris, soft-tissue destruction, thick-walled fluid collections, and associated medial calcar resorption described at MRI [22] (Fig. 10).

Posterior hip dislocation is a potential postoperative complication after total hip arthroplasty placement through a posterior or posterolateral approach. To mitigate this risk, posterior soft-tissue reconstruction is often performed at the time of surgery to enhance hip joint stability [23]. As such, it is imperative to assess the integrity of the posterior joint capsule and short external rotator muscles. Posterior capsular dehiscence can be appreciated at MRI by a lack of continuity of the posterior pseudocapsule and short external rotators with the greater trochanter, often showing a fluid-filled gap interposed between the two, with or without associated anterior pseudocapsular thickening and hyperintensity. Longitudinal MRI studies indicate that the repairs fail early but that the retracted tendons form scar-in-continuity that aligns with the tendon long axis and prevents instability in most cases [23].

A frequent source of anterior hip pain after hip arthroplasty is iliopsoas tendinopathy, which often results from impingement of the iliopsoas tendon by an overly anteverted acetabular cup, oversized acetabular component, or long iliac fixation screws [24]. MRI features of iliopsoas impingement syndrome include tendinosis, partial-thickness tears, and full-thickness tendon rupture, with or without associated iliopsoas or subiliacus bursitis.

After total hip arthroplasty, lateral hip pain is often related to abductor tendinopathy, which ranges from gluteus medius and minimus tendinosis to partial-thickness longitudinal tears to full-thickness tendon tears, with or without associated greater trochanteric bursitis. Acutely,

peritendinous edema may be appreciated within the surrounding soft tissues, whereas in the chronic setting, MRI may show scar formation between the ends of the torn tendon fibers, or to the adjacent pseudocapsule or iliotibial band [4].

Although postoperative infection is a relatively uncommon complication after total hip arthroplasty [25], it often presents a diagnostic dilemma at imaging and frequently requires arthrocentesis to confirm or reject its presence. Several nonspecific MRI features of infection include joint effusion, extracapsular soft-tissue edema, and reactive lymphadenopathy. Findings consistent with a sinus tract, abscess, or osteomyelitis are more specific but less sensitive indications of infection. Finally, a thick lamellated hyperintense synovium composed of multiple layers has been found to be both highly sensitive and specific for infection with high inter- and intraobserver reliability [26].

Conclusion

MRI with refined pulse sequence parameters, metal artifact–reducing techniques, and dedicated sequences allows reliable and reproducible evaluation of the native and postarthroplasty hip joint. It affords identification of aseptic loosening, wear-induced synovitis, and metal arthroplasty–associated complications, which can ultimately lead to arthroplasty failure. In addition, more recent use of dynamic contrast-enhanced MRI allows identification of patients who are at increased risk of developing femoral head osteonecrosis and associated collapse.

Acknowledgments

Supported by grant 1R01 AR064840-01 from the National Institute of Arthritis and Musculoskeletal and Skin Diseases, National Institutes of Health.

H. G. Potter has received research support from GE Healthcare.

References

1. Maradit Kremers H, Larson DR, Crowson CS, et al. Prevalence of total hip and knee replacement in the United States. J Bone Joint Surg Am. 2015; 97:1386–1397. [PubMed: 26333733]
2. Koff MF, Shah P, Potter HG. Clinical implementation of MRI of joint arthroplasty. AJR. 2014; 203:154–161. [PubMed: 24951209]
3. Koff MF, Burge A, Koch KM, Potter HG. Imaging near orthopaedic hardware. J Magn Reson Imaging. 2017 Feb 2. [Epub ahead of print].
4. Fritz J, Lurie B, Miller TT, Potter HG. MR imaging of hip arthroplasty implants. RadioGraphics. 2014; 34:E106–E132. [PubMed: 25019450]
5. Hargreaves BA, Worters PW, Pauly KB, Pauly JM, Koch KM, Gold GE. Metal-induced artifacts in MRI. AJR. 2011; 197:547–555. [PubMed: 21862795]
6. Hayter CL, Koff MF, Potter HG. Magnetic resonance imaging of the postoperative hip. J Magn Reson Imaging. 2012; 35:1013–1025. [PubMed: 22499278]
7. Koff MF, Shah P, Koch L, Potter HG. Quantifying image distortion of orthopedic material in magnetic resonance imaging. J Magn Reson Imaging. 2013; 38:610–618. [PubMed: 23292702]
8. Delfaut EM, Beltran J, Johnson G, Rousseau J, Marchandise X, Cotten A. Fat suppression in MR imaging: techniques and pitfalls. RadioGraphics. 1999; 19:373–382. [PubMed: 10194785]
9. Koch KM, Lorbiecki JE, Hinks RS, King KF. A multispectral three-dimensional acquisition technique for imaging near metal implants. Magn Reson Med. 2009; 61:381–390. [PubMed: 19165901]

10. Lu W, Pauly KB, Gold GE, Pauly JM, Hargreaves BA. SEMAC: slice encoding for metal artifact correction in MRI. Magn Reson Med. 2009; 62:66–76. [PubMed: 19267347]
11. Koch KM, Koff MF, Shah PH, Kanwischer A, Gui D, Potter HG. Flexible longitudinal magnetization contrast in spectrally overlapped 3D-MSI metal artifact reduction sequences: technical considerations and clinical impact. Magn Reson Med. 2015; 74:1349–1355. [PubMed: 25365957]
12. Kaushik A, Sankaran B, Varghese M. Prognostic value of dynamic MRI in assessing post-traumatic femoral head vascularity. Skeletal Radiol. 2009; 38:565–569. [PubMed: 19266195]
13. Dyke JP, Lazaro LE, Hettrich CM, Hentel KD, Helfet DL, Lorich DG. Regional analysis of femoral head perfusion following displaced fractures of the femoral neck. J Magn Reson Imaging. 2015; 41:550–554. [PubMed: 24338938]
14. O'Connor JP, Tofts PS, Miles KS, Parkes LM, Thompson G, Jackson A. Dynamic contrast-enhanced imaging techniques: CT and MRI. Br J Radiol. 2011; 84:S112–S120. [PubMed: 22433822]
15. Sebag G, Ducou Le Pointe D, Klein I, et al. Dynamic gadolinium-enhanced subtraction MR imaging: a simple technique for the early diagnosis of Legg-Calvé-Perthes disease: preliminary results. Pediatr Radiol. 1997; 27:216–220. [PubMed: 9126573]
16. Purdue PE, Koulouvaris P, Potter HG, Nestor BJ, Sulco TP. The cellular and molecular biology of periprosthetic osteolysis. Clin Orthop Relat Res. 2006; 454:251–261.
17. Drummond J, Tran P, Fary C. Metal-on-metal hip arthroplasty: a review of adverse reactions and patient management. J Funct Biomater. 2015; 6:486–499. [PubMed: 26132653]
18. Campbell P, Ebramzadeh E, Nelson S, Takamura K, De Smet K, Amstutz HC. Histological features of pseudotumor-like tissues from metal-on-metal hips. Clin Orthop Relat Res. 2010; 468:2321–2327. [PubMed: 20458645]
19. Nawabi DH, Gold S, Lyman S, Fields K, Padgett DE, Potter HG. MRI predicts ALVAL and tissue damage in metal-on-metal hip arthroplasty. Clin Orthop Relat Res. 2014; 472:471–481. [PubMed: 23354460]
20. Whitehouse MR, Endo M, Zachara S, et al. Adverse local tissue reactions in metal-on-polyethylene total hip arthroplasty due to trunnion corrosion. Bone Joint J. 2015; 97-B:1024–1030. [PubMed: 26224816]
21. Gilbert JL, Sivan S, Liu Y, Kocagöz SB, Arnholt CM, Kurtz SM. Direct in vivo inflammatory cell-induced corrosion of CoCrMo alloy orthopedic implant surfaces. J Biomed Mater Res A. 2015; 103:211–223. [PubMed: 24619511]
22. Burge AJ, Gold SL, Lurie B, et al. MR imaging of adverse local tissue reactions around rejuvenate modular dual-taper stems. Radiology. 2015; 277:142–150. [PubMed: 26030658]
23. McLawhorn AS, Potter HG, Cross MB, et al. Posterior soft tissue repair after primary THA is durable at mid-term followup: a prospective MRI study. Clin Orthop Relat Res. 2015; 473:3183–3189. [PubMed: 26047646]
24. Bricteux S, Beguin L, Fessy MH. Iliopsoas impingement in 12 patients with a total hip arthroplasty [in French]. Rev Chir Orthop Reparatrice Appar Mot. 2001; 87:820–825. [PubMed: 11845086]
25. Pulido L, Ghanem E, Joshi A, Purtill JJ, Parvizi J. Periprosthetic joint infection: the incidence, timing, and predisposing factors. Clin Orthop Relat Res. 2008; 466:1710–1715. [PubMed: 18421542]
26. Plodkowski AJ, Hayter CL, Miller TT, Nguyen JT, Potter HG. Lamellated hyperintense synovitis: potential MR imaging sign of an infected knee arthroplasty. Radiology. 2013; 266:256–260. [PubMed: 23091176]

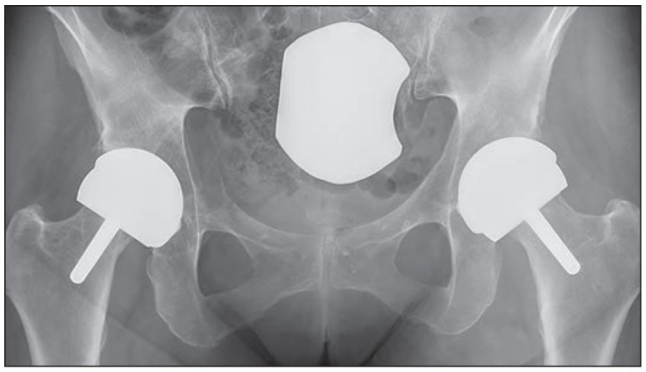

A

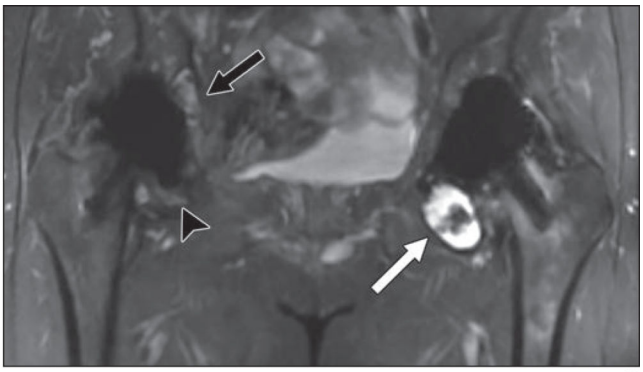

B

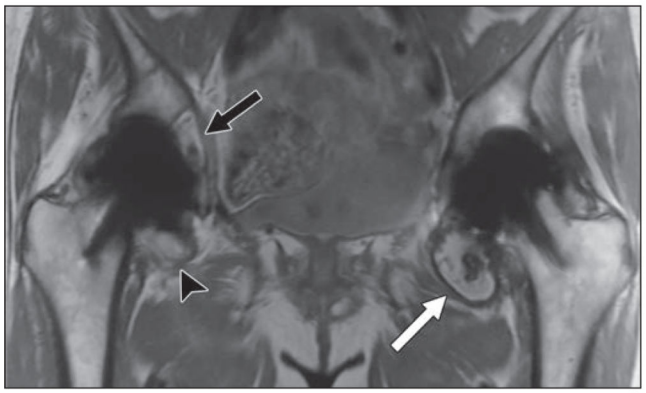

C

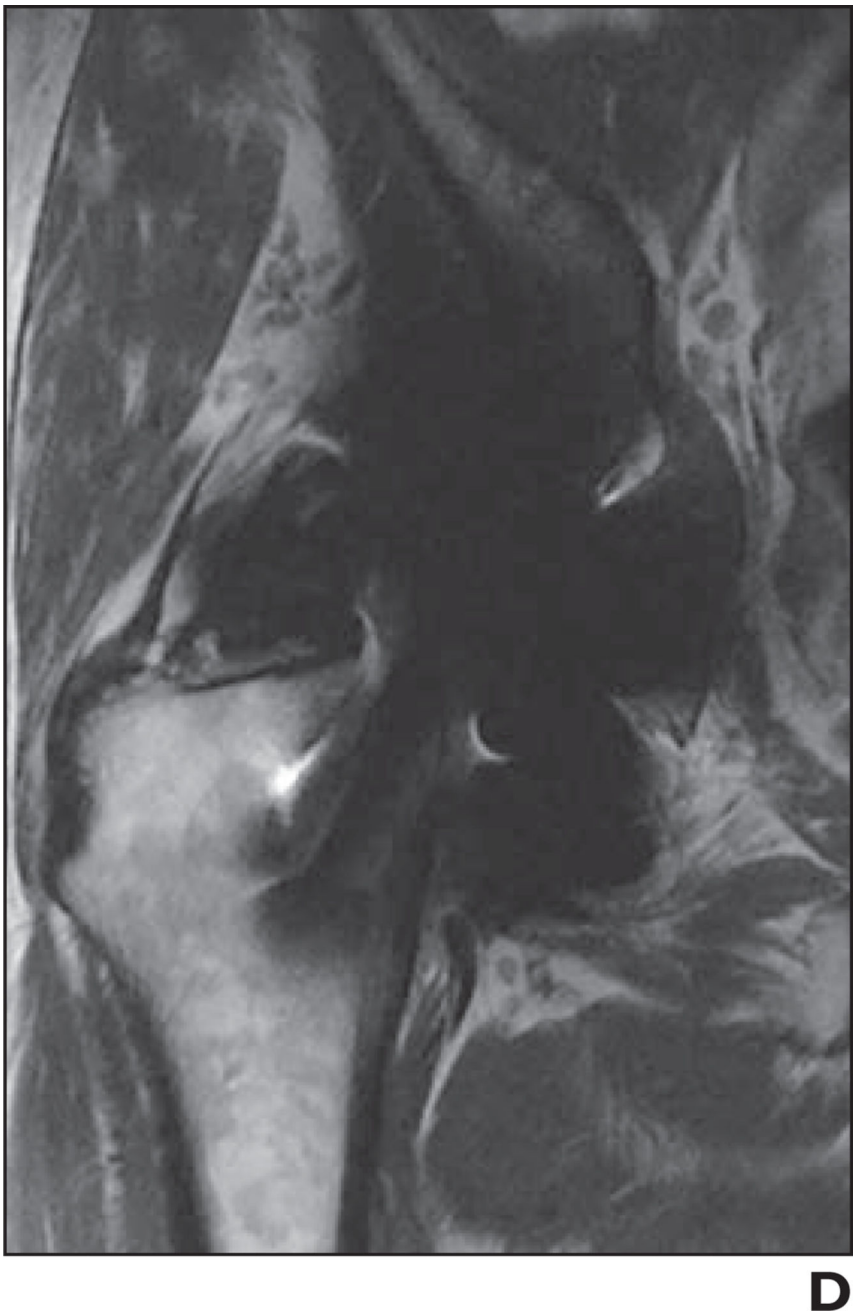

Fig. 1.

61-year-old woman who underwent bilateral resurfacing arthroplasty using Birmingham hip components (Smith & Nephew), reportedly 6 years previously on right and 3 years previously on left.

A, Anteroposterior radiograph shows no abnormalities.

B and **C,** Coronal multiacquisition variable-resonance image combination (MAVRIC) inversion recovery (**B**) and MAVRIC proton density–weighted (**C**) MR images show posterior column osteolysis on right (*black arrows*). Note thickened inferomedial synovial

lining on right (*arrowheads*), indicative of adverse tissue reaction. On left, there is thinner synovial reaction with low-signal-intensity debris, indicative of metallosis (*white arrows*). 61-year-old woman who underwent bilateral resurfacing arthroplasty using Birmingham hip components (Smith & Nephew), reportedly 6 years previously on right and 3 years previously on left.

D, Coronal fast spin-echo MR image shows abductors, but adverse local tissue reaction occurring in inferomedial recess and acetabular bone loss are completely obscured.

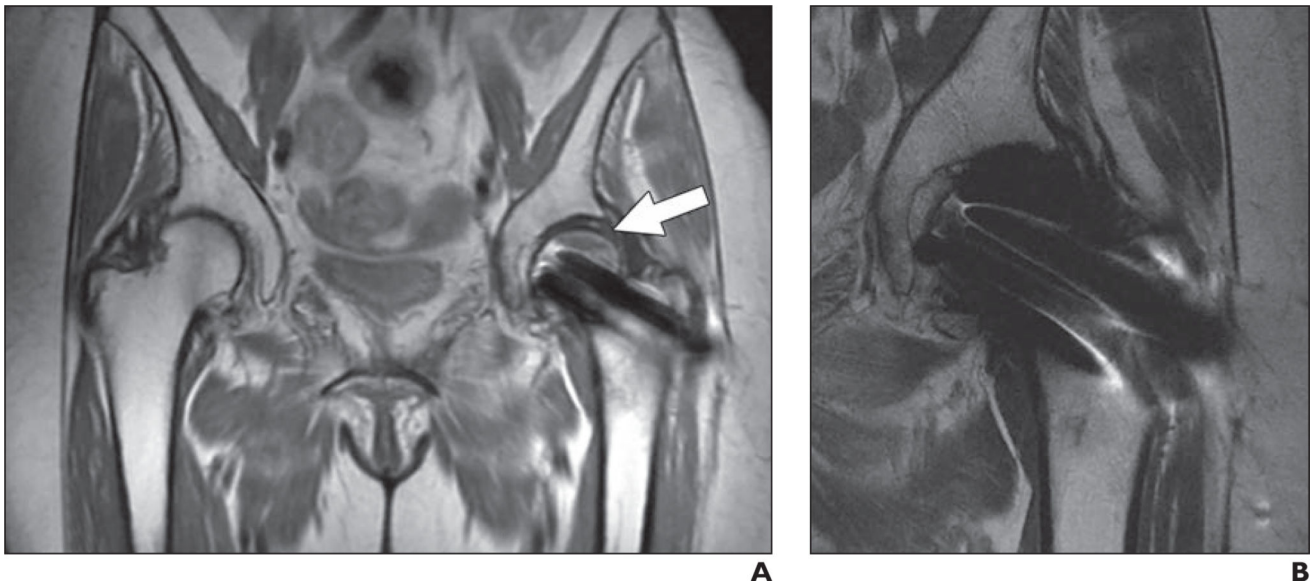

Fig. 2.

72-year-old woman who presented with pain 10 months after cannulated screw fixation of impacted femoral neck fracture.

A and **B,** Coronal proton density–weighted fast spin-echo multiacquisition variable-resonance image combination (MAVRIC) MR image (**A**) shows osteonecrosis of superior portion of femoral head without associated subchondral collapse (*arrow*), which could not be appreciated on non-MAVRIC proton density–weighted fast spin-echo pulse sequence (**B**).

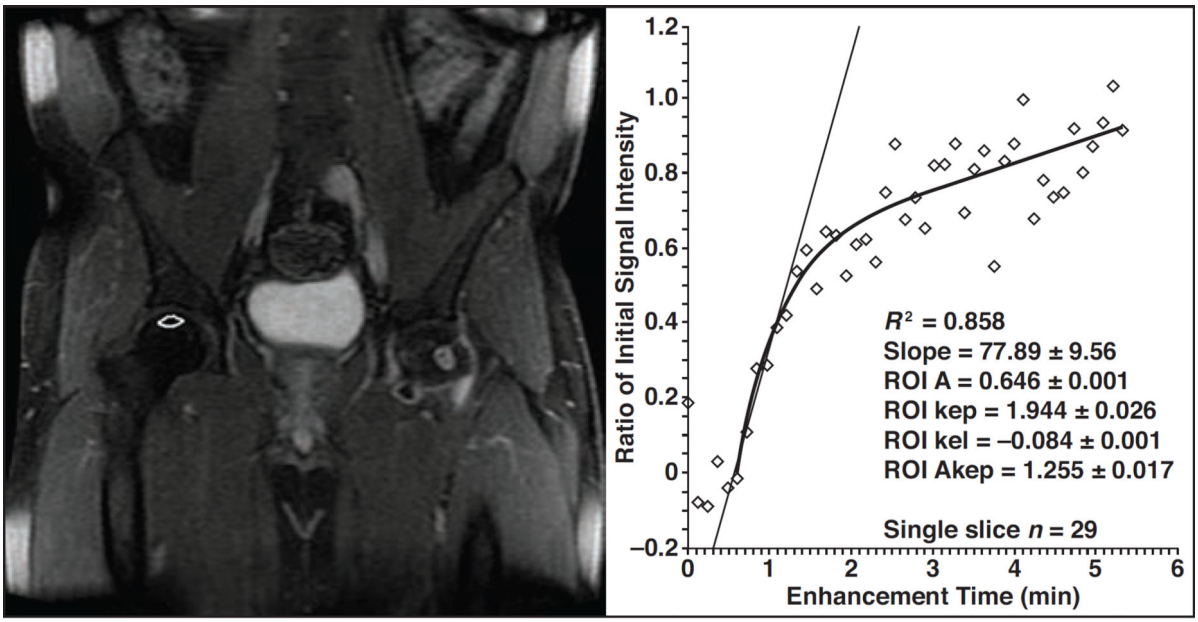

Fig. 3.

37-year-old man with 1-year history of prednisone use in 2013 who presented with right groin pain.

A and **B,** Dynamic contrast-enhanced MR images of right femoral head (**A**) and acetabulum (**B**) are presented with slice and ROIs (*white outlines*) delineated on left and time history for enhancement shown on right. Control study of right acetabulum (**B**) shows rapid increase in contrast enhancement with slope of 0.859 and normal washout, whereas ischemic right femoral head enhancement curve (**A**) shows rate of increase of 0.858 with delayed washout, reflective of associated reparative response. Diamonds in graphs denote average

enhancement of all voxels in ROI at indicated time point. Lines in graph denote estimate of rate of enhancement. Curves are fit of time history of enhancement. Kep, kel, and Akep are pharmacokinetic parameters of model used by code to describe various parameters of uptake and elimination of gadolinium contrast material.

Fig. 4.

65-year-old man who presented with groin pain. Coronal proton density–weighted fast spin-echo MR image shows well-integrated total hip arthroplasty with sharp interface (*arrow*) between bone and arthroplasty.

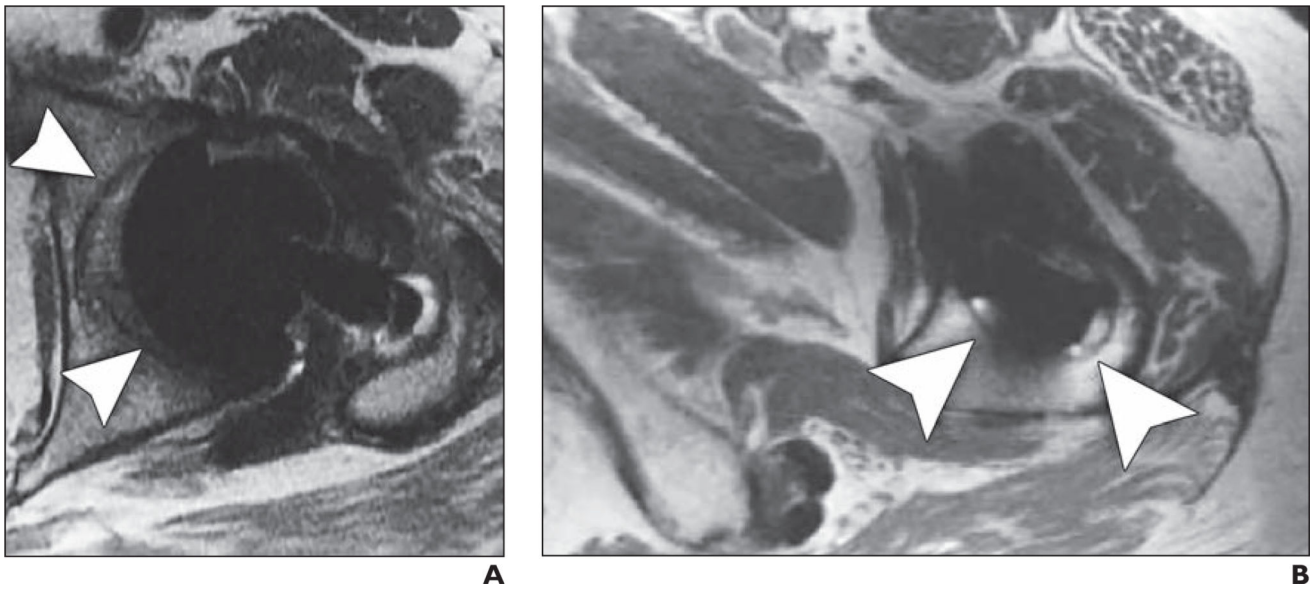

Fig. 5.

60-year-old woman who presented with hip pain.

A and **B,** Axial proton density–weighted fast spin-echo MR images show thin rim of intermediate signal intensity (*arrowheads*) around acetabular (**A**) and femoral (**B**) components, consistent with fibrous membrane formation.

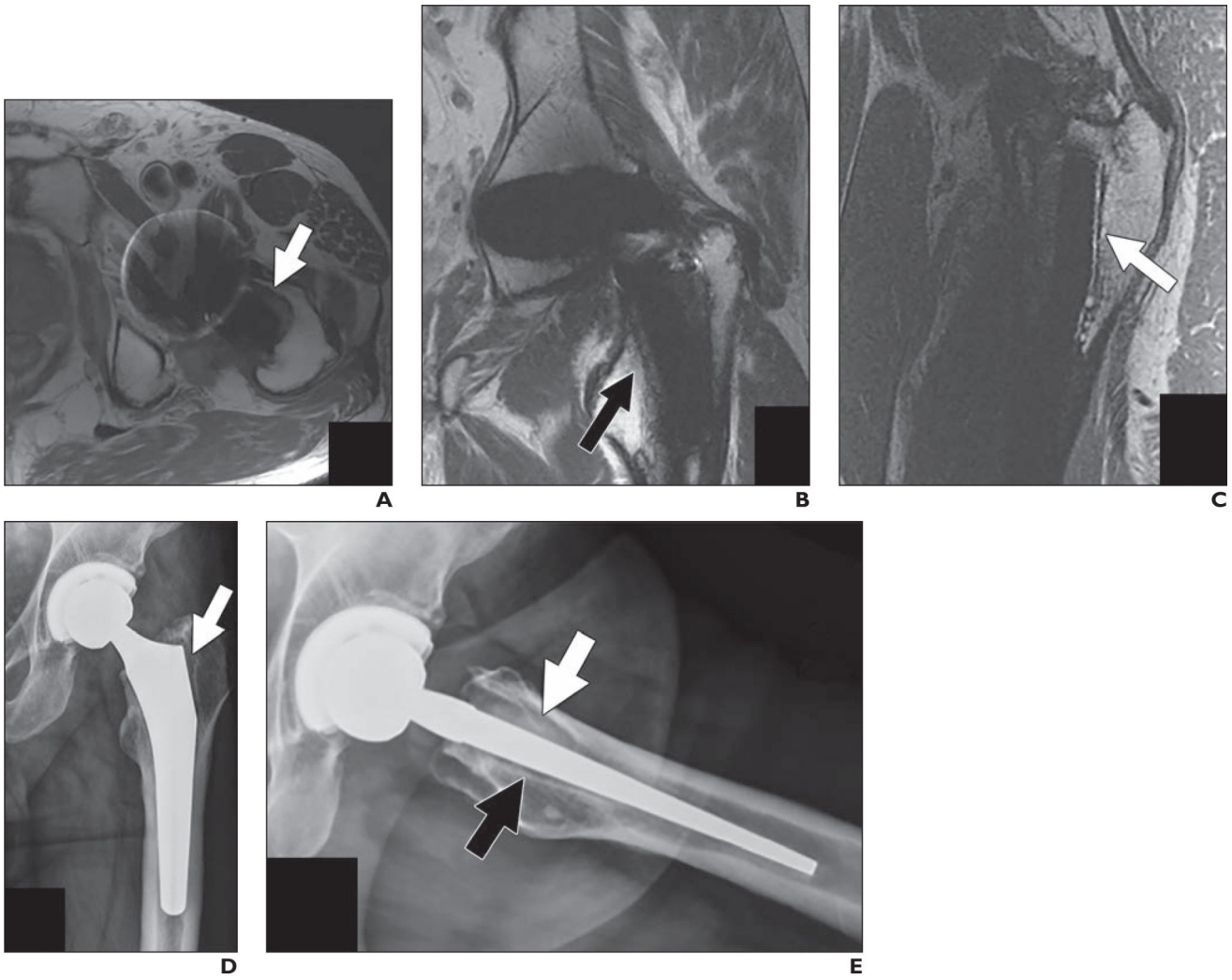

Fig. 6.

67-year-old man who presented with proximal thigh pain 18 months after modular metallic hip arthroplasty placement performed at outside institution.

A–C, Axial (**A**), coronal (**B**), and sagittal (**C**) proton density–weighted fast spin-echo MR images show osteolysis in Gruen zone 8 (*arrow*, **A**), zone 7 (*arrow*, **B**), and zone 14 (*arrow*, **C**).

D and **E,** Corresponding anteroposterior (**D**) and frog lateral (**E**) radiographs of left hip show resorption around proximal femur in region of porous coat with radiolucency in Gruen zone 1 (*arrow*, **D**), zone 8 (*white arrow*, **E**), and zone 14 (*black arrow*, **E**). Tissue obtained at time of femoral component revision showed fibrinous exudate at bone-implant interface with intraoperative cultures negative for infection.

Fig. 7.

58-year-old man who presented with pain 10 years after ceramic-on-polyethylene total hip arthroplasty placement. Coronal proton density–weighted fast spin-echo MR image shows eccentric positioning of femoral head within acetabular cup (*black arrow*) and associated bulky synovitis with low-signal-intensity debris expanding capsule (*arrowhead*), consistent with polyethylene wear and associated polymeric reaction. Note associated osteolysis in Gruen zone 7 (*white arrow*).

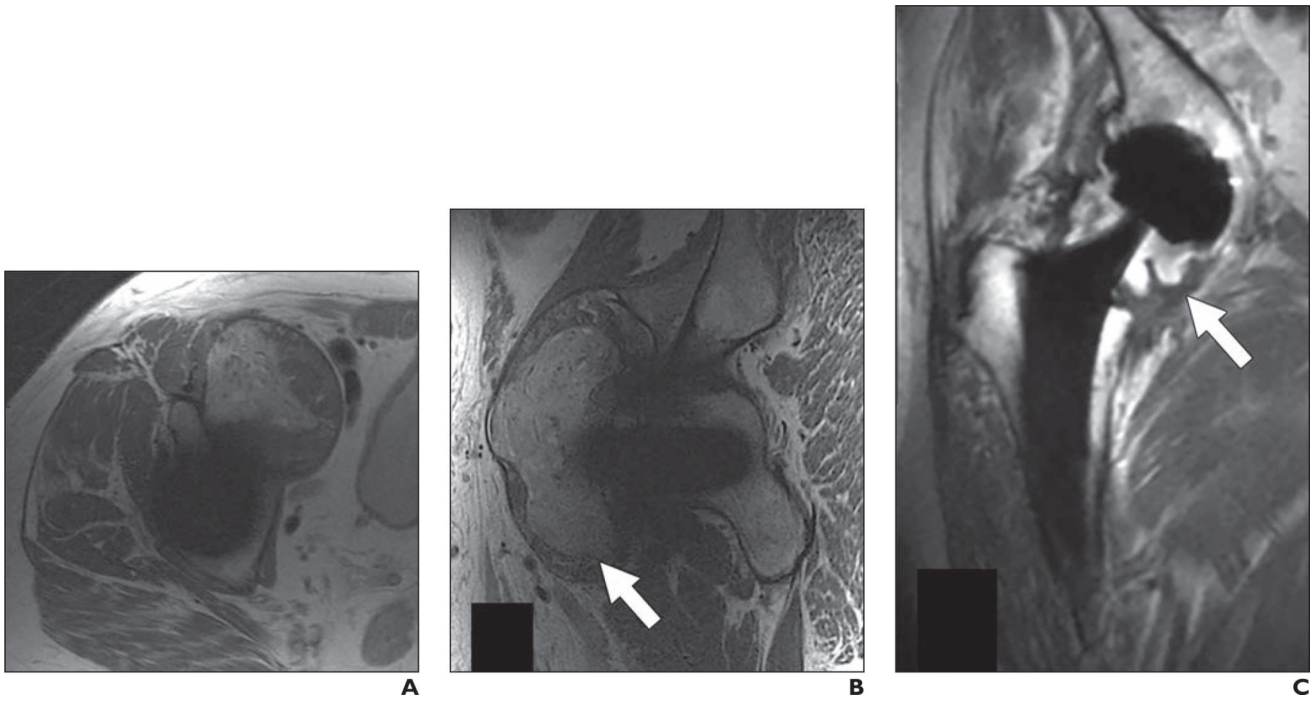

Fig. 8.

66-year-old man who presented with periodic right hip pain 10 years after metal-on-metal hip arthroplasty placement.

A and **B,** Axial (**A**) and sagittal (**B**) proton density–weighted fast spin-echo MR images show marked synovial expansion and synovitis containing prominent intermediate- and low-signal-intensity debris decompressing superiorly into iliopsoas and subiliacus bursae (*arrow*, **B**), indicating adverse local tissue reaction with component of metallosis.

C, Note thickened inferomedial recess lining (*arrow*) on coronal proton density–weighted fast spin-echo multiacquisition variable-resonance combination MR image.

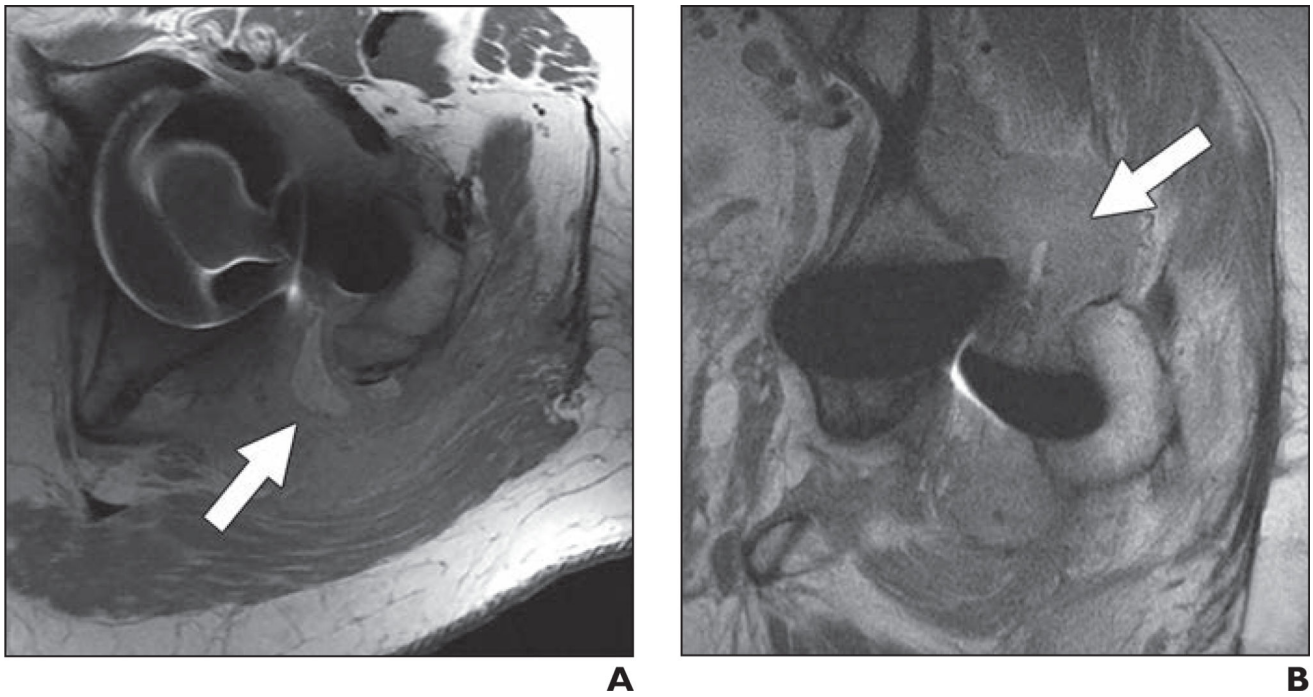

Fig. 9.

62-year-old man who presented with pain 1 year after placement of recalled metal-on-metal hip arthroplasty.

A and **B,** Axial (**A**) and coronal (**B**) proton density–weighted fast spin-echo MR images show massive distention of hip pseudocapsule with markedly thickened rind (*arrows*), dehiscence of lateral margin of posterior capsular repair, and extension into greater trochanteric bursa, consistent with aggressive adverse local tissue reaction.

Fig. 10.

60-year-old man who presented with pain approximately 1 year after right hip arthroplasty placement. Coronal proton density–weighted fast spin-echo MR image shows intracapsular expansion, creating indolent pattern of erosion within Gruen zone 8 and extending to top of Gruen zone 7 (*arrow*), reflecting early adverse local tissue reaction related to trunnionosis.

TABLE 1

Recommended Protocols for MRI of Total Hip Arthroplasty, by Imaging Plane and Sequence Used

Parameter	Coronal MAVRIC Inversion Recovery (Whole Pelvis)	Coronal MAVRIC FSE (Whole Pelvis)	Axial FSE (Whole Pelvis)	Sagittal FSE (Affected Hip)	Coronal FSE (Affected Hip)	Oblique Axial FSE (Affected Hip)
TR (ms)	4000	4000	5500	5500	4100	4000
TE (ms)			24	24	24	24
Inversion time (ms)	150					
Bandwidth (kHz)			125	125	125	125
Echo-train length	24	24	14	21	24	20
Flip angle (°)	110	110	160	160	160	160
No. of excitations			3	4	5	4
FOV (cm)	36	36	32	26	26	26
Matrix	256 × 192	512 × 256	512 × 256	512 × 384	512 × 352	512 × 256
Slice/gap (mm)	5.5	3.5	5/0	2.5/0	4/0	4/0
No phase wrap	No	No	Yes	Yes	Yes	Yes

Note—Patients were imaged in the supine position, with the feet first. MAVRIC = multiacquisition variable-resonance image combination, FSE = fast spin-echo.

TABLE 2

Recommended Dynamic Contrast-Enhanced Hip MRI Perfusion Protocol

Parameter	Value
TR (ms)	
Bandwidth (kHz)	62.5
Echo-train length	
Flip angle (°)	12
No. of excitations	1
FOV (cm)	40
Matrix	256 × 128
Slice/gap (mm)	4

Note—All images were acquired in the coronal plane using the liver acquisition with volume acceleration technique and a cardiac coil. Patients were imaged in the supine position, with the feet first.